Full-Band Quantum Simulations of Semiconductor Devices based on Empirical Pseudopotential Hamiltonians in the presence of Phonon Scattering and Non-Radiative Recombination

Alessandro Pilotto, Adel M'Foukh, Philippe Dollfus, Jérôme Saint-Martin, and Marco G. Pala
Université Paris-Saclay, CNRS, C2N, 10 Boulevard Thomas Gobert, 91120 Palaiseau, France.
email: alessandro.pilotto@universite-paris-saclay.fr, marco.pala@c2n.upsaclay.fr

***Abstract*—We present a full-band quantum transport model based on the Empirical Pseudopotential Method (EPM) that includes electron-phonon scattering and Shockley-Read-Hall (SRH) recombination via non-radiative multiphonon relaxation. The model has been used to simulate the current-voltage characteristics of two different Silicon-based devices and it shows that a) in a p-i-n diode, SRH recombination gives the dominant contribution to the OFF-state current of the junction, while phonon scattering is responsible for the degradation of the current in the ON-state; b) the inclusion of SRH recombination in the simulation of an Esaki tunneling diode predicts a reduction of the peak-to-valley current ratio, while phonon scattering enhances indirect tunneling transitions from the valence band in Γ to the conduction band minima in the Δ valleys that are not located along the transport direction.**

***Index Terms*—NEGF, Empirical Pseudopotential Method, Shockley-Read-Hall Recombination, Electron-Phonon Interaction**

I. Introduction

A quantum transport formalism based on full-band hamiltonians is necessary to overcome the limitations of approximated models, such as the effective mass approximation and the $\mathbf{k}\cdot\mathbf{p}$ method, in describing band-to-band transitions, especially for indirect band gap materials like Silicon. In recent years, the EPM [1] has been proven successful to describe full-band energy effects in Non-Equilibrium Green's Function (NEGF) simulations [2], [3].

In order to realistically simulate semiconductor devices, this abstract presents NEGF simulations based on EPM hamiltonians in the presence of electron-phonon interaction and Shockley-Read-Hall recombination via non-radiative multiphonon relaxation [4]. Simulations of Silicon junctions are presented to illustrate the method.

The paper proceeds as follows. The details of the full-band quantum transport model based on the Empirical Pseudopotential Method are given in Section II. The results of the simulations of two Silicon-based devices, a p-i-n diode and an Esaki tunneling junction [5], are presented and discussed in Section III. Finally, our concluding remarks are reported in Section IV.

II. Quantum Transport

The transport formalism used in this work is the one of the NEGF method and all the simulations have been performed by using the Green-Tea solver [6], that relies on pseudopotential hamiltonians described on a basis set composed of unit-cell restricted Bloch functions (URBFs) $\{\Phi_{n,k_x}(\mathbf{k}_{yz})\}$. Here, we considered the conventional unit cell of Silicon (i.e. the cube with side of length a_0 and containing 8 atoms, see Fig. 1(a)) as the unit cell for transport calculations.

For a given transverse wavevector $\mathbf{k}_{yz} = (k_y, k_z)$, the EPM hamiltonian has been computed by using the form factors of [7] and then discretized in the hybrid space by using the methodology proposed in [2].

Finally, the hamiltonian has been projected onto the URBF basis set, obtained by sampling k_x in the unit cell at the values $k_x = [0; 0.5] \times 2\pi/a_0$. The agreement for $\mathbf{k}_{yz} = [0; 0]$ between the band structure computed in the URBF basis, when 56 functions were used (32 for the valence band states and the remaining for the conduction band states), and the one computed in the plane-wave (PW) basis is shown in Fig. 1(b).

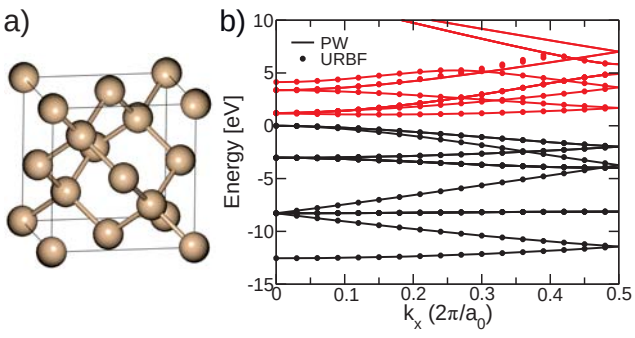

Fig. 1. (a) Cubic unit cell of Silicon with 8 atoms. (b) Band structure of the 8-atom unit cell of Silicon of subplot (a) computed with the EPM along the k_x direction for $\mathbf{k}_{yz} = [0; 0]$. The results obtained by using a PW basis set (lines) are compared to the ones obtained by using the URBF basis set (dots).

Physical quantities (current, charge, etc.) were finally computed by a self-consistent solution of the NEGF equations

(coupled with the solution of the 3D non-linear Poisson equation for the electrostatics).

A. Electron-phonon self-energies

Electron-phonon (el-ph) interaction has been included by using self-energies expressed within the self-consistent Born approximation. The elastic and energy equi-partition approximation has been used to describe scattering with acoustic phonons, whereas optical phonons have been described by a single effective phonon frequency. For each cell along the transport direction, the electron-phonon self-energies in the URBF basis can be expressed in a matrix notation as

$$\Sigma^{<,\mathrm{ac}}(\mathbf{k}_{yz};E) = \frac{D_{\mathrm{ac}}^2 k_B T}{\rho v_s^2} \times \sum_{\mathbf{q}_{yz}} S(\mathbf{k}_{yz}-\mathbf{q}_{yz}) G^{<}(\mathbf{k}_{yz}-\mathbf{q}_{yz};E)\, S^{\dagger}(\mathbf{k}_{yz}-\mathbf{q}_{yz}) \tag{1}$$

$$\Sigma^{<,\mathrm{op}}(\mathbf{k}_{yz};E) = \frac{\hbar D_{\mathrm{op}}^2}{2\rho\Omega_0}\left[N_{\Omega_0}+\frac{1}{2}\pm\frac{1}{2}\right] \times \sum_{\mathbf{q}_{yz}} S(\mathbf{k}_{yz}-\mathbf{q}_{yz}) G^{<}(\mathbf{k}_{yz}-\mathbf{q}_{yz};E\pm\hbar\Omega_0)\, S^{\dagger}(\mathbf{k}_{yz}-\mathbf{q}_{yz}) \tag{2}$$

where $S(\mathbf{k}_{yz})$ is an overlap integral matrix involving the $\{\Phi_{n,k_x}(\mathbf{k}_{yz})\}$, k_B is the Boltzmann constant, T is the temperature, ρ is the density, $v_s = (2v_t + v_l)/3$ is the average sound velocity (t and l denote the transverse and longitudinal directions, respectively), $N_{\Omega_0} = [\exp(\hbar\Omega_0/K_BT)-1]^{-1}$ is the occupation number for the phonon with frequency Ω_0, and D_{ac} and and D_{op} are the deformation potentials for scattering with acoustic and optical phonons, respectively.

We adopted similar expressions for the lesser-than self-energy $\Sigma^{>}$, while the retarded self-energy was approximated by considering it equal to its anti-hermitian part: $\Sigma \approx [\Sigma^{>} - \Sigma^{<}]/2$.

The values of the parameters for Silicon used to describe electron-phonon scattering in this work have been taken from [8] and are reported in Tab. I.

	D_{ac} [eV]	D_{op} [eV/cm]	$\hbar\Omega_0$ [meV]	ρ [g/cm^3]	v_t [cm/s]	v_l [cm/s]
CBs	5.2	2.5×10^8	60	2.33	5.41×10^5	9×10^5
VBs	10.8	6.6×10^8				

TABLE I
EL-PH SCATTERING PARAMETERS FOR SI USED IN THIS WORK (FROM [8]). CBS AND VBS STAND FOR CONDUCTION BANDS AND VALENCE BANDS, RESPECTIVELY.

B. SRH Recombination via Non-Radiative Multiphonon Relaxation

SRH recombination via non-radiative multiphonon relaxation [4] has been included in NEGF calculations by using the model of [9], which assumes that the defect density is strongly localized in space and energy. The lesser-than and greater-than Green's function of the defect, $G_d^{<}$ and $G_d^{>}$, were computed by using the quasi-equilibrium expressions $G_d^{<}(E) = i f_d(E) A_d(E)$, and $G_d^{>}(E) = -i[1-f_d(E)]A_d(E)$, where $A_d(E) = 2\pi\delta(E-E_{\mathrm{def}})$ is the defect's spectral function and f_d describes the defect's occupation. The value of $f_d(E=E_{\mathrm{def}})$ is given by the balance at steady-state between the capture and emission rates [9], namely

$$f_d(E=E_{\mathrm{def}}) = -i\frac{\Sigma_{dc}^{<}(E_{\mathrm{def}})+\Sigma_{dv}^{<}(E_{\mathrm{def}})}{\Gamma_{dc}(E_{\mathrm{def}})+\Gamma_{dv}(E_{\mathrm{def}})}, \tag{3}$$

where $\Gamma \equiv i(\Sigma^{>}-\Sigma^{<})$.

For the conduction bands, the self-energies describing carrier capture/emission into/from the defect state and into/from the bands were computed with the following equations derived from [9]–[11]

$$\Sigma_{dc}^{\lessgtr}(x_{\mathrm{def}};E) = \frac{1}{\mathcal{A}}\sum_{\mathbf{k}_{yz}}\sum_{l\geq 0}\mathcal{M}_{\mathrm{em/capt}}(l) \times G_c^{\lessgtr}(\mathbf{k}_{yz},x_{\mathrm{def}},x_{\mathrm{def}};E+l\hbar\Omega_0) \tag{4}$$

$$\Sigma_{cd}^{\lessgtr}(\mathbf{k}_{yz},x_{\mathrm{def}};E) = \rho_d\sum_{l\geq 0}\mathcal{M}_{\mathrm{em/capt}}(l) G_d^{\lessgtr}(E-l\hbar\Omega_0) S(\mathbf{k}_{yz}) \tag{5}$$

$$\mathcal{M}_{\mathrm{capt}}(l) = \mathcal{M}_{dc}^0 \frac{(l-S_{HR})^2}{S_{HR}} e^{-S_{HR}(2N_{\Omega_0}+1)}\left(\frac{N_{\Omega_0}+1}{N_{\Omega_0}}\right)^{l/2} \times \mathcal{I}_l(2S_{HR}\sqrt{N_{\Omega_0}(N_{\Omega_0}+1)}) \tag{6}$$

where the subscript c identifies the conduction bands, ρ_d is the defects' density, l is the number of phonons involved in the recombination process, S_{HR} is the Huang-Rhys factor ($S_{HR}=3.5$ in this work), $\mathcal{I}_l$ is the modified Bessel function of l-th order. We remark that the self-energy in Eq. (4) is calculated by using the real space Green's function for the conduction band states $G_c^{\lessgtr}(\mathbf{k}_{yz},x,x';E)$. On the other hand, the matrix of the overlap integral of the Bloch functions, $S(\mathbf{k}_{yz})$, has been exploited to reformulate the self-energies of Eq. (5) in the URBF basis.

The constant $\mathcal{M}_{dc}^0$ is linked to the capture cross sections ($\sigma_{n,p}$) as described in [12]:

$$\mathcal{M}_{dc}^0 = (4\pi)^2 r_{t1}^3 \frac{D_{\mathrm{op}}^2\hbar}{\rho\Omega_0 a_0^3} q_0^2 \frac{\hbar^2}{2E_t m_e}, \tag{7}$$

where $r_{t1} = \sqrt{\sigma_n/\pi}$ is the localization radius of the trap state at energy E_t, D_{op} and Ω_0 are the deformation potential for scattering with optical phonons and the optical phonon energy (see Tab. I), respectively, ρ is the density, a_0 is the lattice constant, q_0 is the phonon wave number (we have assumed $q_0 = 2\pi/a_0$), and m_e is the electron effective mass.

Finally, the detailed balance at the equilibrium makes possible to write the matrix element for electron emission as a function of the one for electron capture [4], [9], namely

$$\mathcal{M}_{\mathrm{em}}(l) = \mathcal{M}_{\mathrm{capt}}(l) e^{\frac{-l\hbar\Omega_0}{k_B T}}. \tag{8}$$

Similar expressions were used to describe the coupling between the trap state and the valence bands and again the retarded self-energy was approximated as $\Sigma \approx [\Sigma^{>}-\Sigma^{<}]/2$.

III. Results

In this Section, we present the results obtained by simulating two different Silicon-based diodes with the full-band quantum transport model described in Section II. In the following, we have always assumed a midgap trap state located in the middle of the active region of the examined devices.

A. p-i-n diode

First, we considered a Silicon p-i-n junction consisting in 10 nm-long contact regions with doping concentration $N_D = N_A = 10^{19}$ cm^{-3} separated by a $L = 10$ nm-thick intrinsic region.

The $I-V$ characteristic under different simulation conditions is reported in Fig. 2. As expected, we notice that SRH recombination is the dominant contribution to the OFF-state current (i.e. for $V < 0.5$ V), as the slope of the $I-V$ curve deviates from 60 mV/dec and approaches the value of 120 mV/dec. The effect of SRH recombination on the current that flows through the diode is also clearly visible from the spectral current density plots at $V = 0.4$ V in Fig. 3.

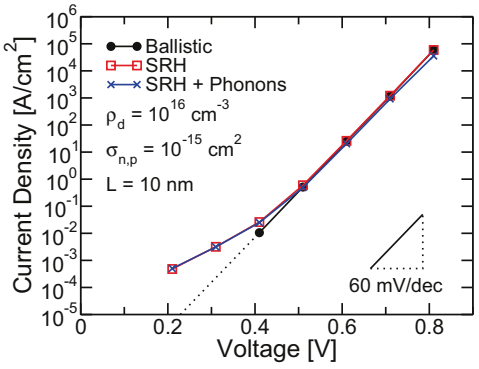

Fig. 2. Current-voltage characteristic of a 10 nm-thick Silicon p-i-n diode in ballistic conditions (black circles), and when SRH recombination (red squares) or SRH recombination and phonon scattering (blue crosses) are included in the simulations. For SRH: $\rho_d = 10^{16}$ cm^{-3}, $\sigma_{n,p} = 10^{-15}$ cm^2.

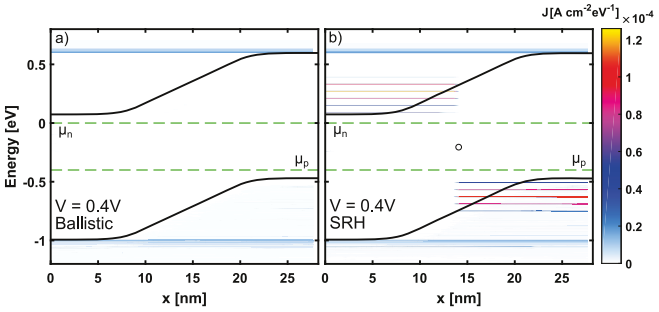

Fig. 3. Spectral current density in a Silicon p-i-n diode at $V = 0.4$V: the n-contact is on the left, the p-contact is on the right. (a) Ballistic conditions; (b) SRH recombination is included in the simulations, the trap location is highlighted with a black circle.

On the other hand, phonon scattering reduces the current, w.r.t. the ballistic case, at high applied bias voltages. This is shown in Fig. 4, where we see that the spectral current at $V = 0.8$ V relaxes towards the band edge when phonon scattering is included in the quantum transport simulations.

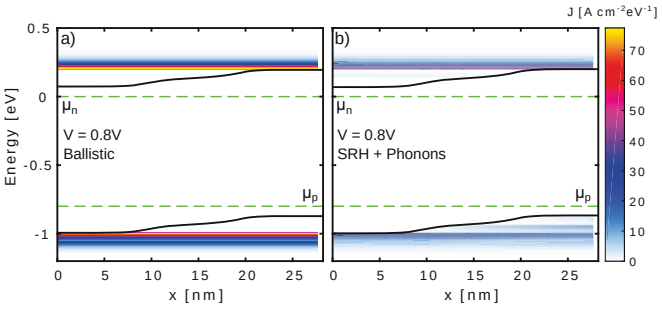

Fig. 4. Spectral current density in a Silicon p-i-n diode at $V = 0.8$V: the n-contact is on the left, the p-contact is on the right. (a) Ballistic conditions; (b) SRH recombination and el-ph interaction are included in the simulations.

B. Esaki tunneling junction

The second device that we simulated is a silicon Esaki tunneling junction [5] featuring 10 nm-long contact regions $N_D = N_A = 5 \times 10^{20}$ cm^{-3} separated by a $L = 4$ nm-thick intrinsic region.

The comparison between the current-voltage curve obtained in the ballistic case and the one with the SRH recombination is shown in Fig. 5. We notice that, by including trap-assisted recombination we obtain a non-null valley current that translates into a peak-to-valley current ratio (PVCR) of about 4.47. This means that SRH recombination permits to recover realistic values of the PVCR: for instance, the PVCR of the Si Esaki diodes experimentally measured in Ref. [13] is 3.94. Figure 6 reports the comparison between the ballistic spectral current density and the one obtained by including el-ph interaction and SRH recombination at $V = 0.185$ V, that corresponds to the valley current minimum. The contribution to the total current given by SRH recombination is visible in plot (b).

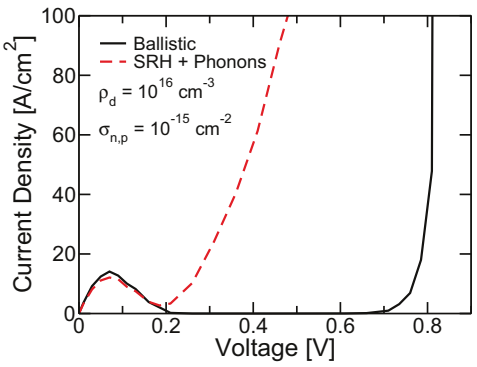

Fig. 5. Current-voltage characteristic of a Silicon Esaki tunneling diode in ballistic conditions (black-solid) and when SRH recombination and phonon scattering are included (red-dashed). For SRH: $\rho_d = 10^{16}$ cm^{-3}, $\sigma_{n,p} = 10^{-15}$ cm^2.

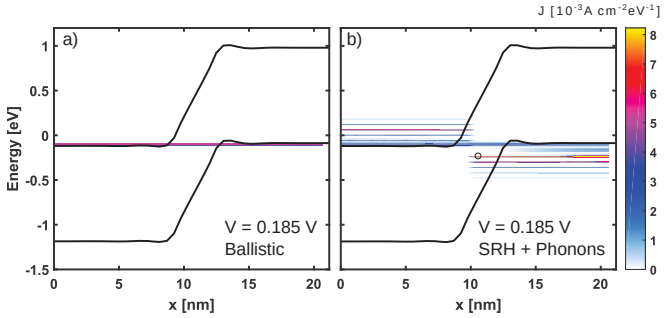

Fig. 6. Spectral current densities in the Esaki tunneling junction of Fig. 5 at $V = 0.185$ V (at the valley current minimum). (a) Ballistic conditions; (b) SRH recombination and phonon scattering are included in the simulations.

By analyzing the density current spectra in Fig. 7, we can also see that the inclusion of phonon scattering reduces the value of the current that flows through the diode, and enhances the coupling between different transverse $\mathbf{k}$-vectors. In fact, while in ballistic conditions the tunneling current is visible only along $\mathbf{k}_{yz} = [0, 0]$ (Figs. 7(a) and (c)), the inclusion of el-ph interaction induces a non-zero spectral current density also for $\mathbf{k}_{yz}$ values corresponding to indirect tunneling from the valence band maximum in Γ to the conduction band minima in Δ valleys (Figs. 7(b) and (d)).

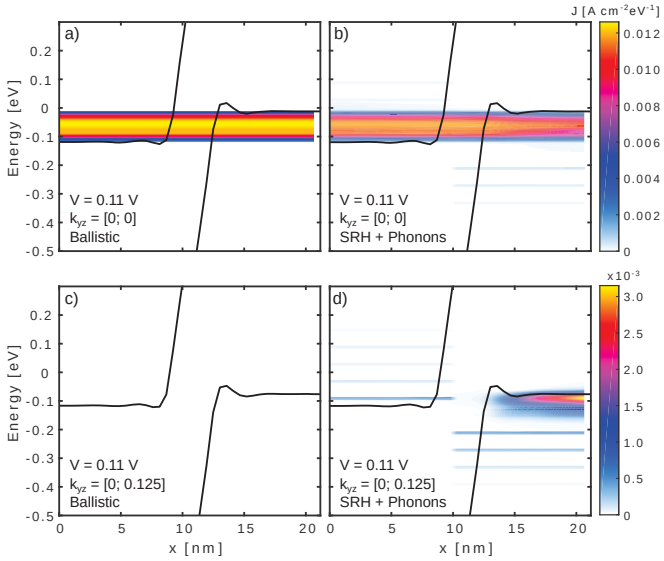

Fig. 7. (a)-(d) Spectral current densities, for different transverse wavevectors, in the Esaki tunneling junction of Fig. 5 at $V = 0.11$ V (at the peak-current) in (a),(c) ballistic conditions and (b),(d) when SRH recombination and el-ph scattering are considered: (a),(b) $\mathbf{k}_{yz} = [0; 0]$; (c),(d) $\mathbf{k}_{yz} = [0; 0.125]$. The n^+-contact is on the left, while the p^+-contact is on the right.

IV. Conclusions

We have performed quantum transport simulations of Silicon junctions based on full-band hamiltonians obtained by using the Empirical Pseudopotential Method and by including phonon scattering and SRH recombination via multiphonon relaxation. While SRH is the dominant contribution to the OFF-current of the diode and degrades the PVCR of the tunneling junction, phonon scattering has the effect of decreasing the current in the ON-state and of coupling wavevectors along different directions. The use of full-band hamiltonians allows us to clearly see the aforementioned phenomena also in indirect gap materials.

V. Acknowledgments

This work was supported by the French "Agence Nationale de la Recherche" through the projects "GeSPAD" (ANR-20-CE24-0004) and "Tunne2D" (ANR-21-CE24-0030).

References

[1] M.L. Cohen and J.R. Chelikowsky, "Electronic structure and optical properties of semiconductors", Springer Series in Solid-State Sciences, Springer Berlin, 1988, doi: 10.1007/978-3-642-97080-1.

[2] M.G. Pala and D. Esseni, "Full-band quantum simulation of electron devices with the pseudopotential method: Theory, implementation, and applications", in Phys. Rev. B 97, 125310, 2018, doi: 10.1103/PhysRevB.97.125310.

[3] A. M'foukh, M.G. Pala and D. Esseni, "Full-Band Quantum Transport of Heterojunction Electron Devices With Empirical Pseudopotentials", IEEE Trans. Elec. Dev. 67 (12), pp. 5662-5668, 2020, doi: 10.1109/TED.2020.3029548.

[4] A. Schenk, "An improved approach to the Shockley–Read–Hall recombination in inhomogeneous fields of space-charge regions", in Journal of Applied Physics 71(7), pp. 3339–3349, 1992, doi: 10.1063/1.350929.

[5] L. Esaki, "New phenomenon in narrow Germanium p-n junctions", in Phys. Rev. 109, 603, 1958, doi: 10.1103/PhysRev.109.603.

[6] M.G. Pala, P. Giannozzi and D. Esseni, "Unit cell restricted Bloch functions basis for first-principle transport models: Theory and application", in Phys. Rev. B 102, 045410, 2020, doi: 10.1103/PhysRevB.102.045410.

[7] M.V. Fischetti, "Monte Carlo simulation of transport in technologically significant semiconductors of the diamond and zinc-blende structures. I. Homogeneous transport", in IEEE Transactions on Electron Devices, vol. 38, no. 3, pp. 364-649, 1991, doi: 10.1109/16.75176.

[8] M.V. Fischetti, N. Sano, S.E. Laux and K. Natori, "Full-band-structure theory of high-field transport and impact ionization of electrons and holes in Ge, Si, and GaAs", in Journal of Technology Computer Aided Design TCAD, pp. 1-50, 1996, doi: 10.1109/TCAD.1996.6449160.

[9] U. Aeberhard, "Nonequilibrium Green's function picture of nonradiative recombination of the Shockley-Read-Hall type", in Phys. Rev. B 99, 125302, 2019, doi: 10.1103/PhysRevB.99.125302.

[10] J.A.G Montoya, A. Tibaldi, C. De Santi, M. Meneghini, M. Goano, F. Bertazzi, "Nonequilibrium Green's function modeling of trap-assisted tunneling in $In_xGa_{1-x}N$/GaN light-emitting diodes", in Phys. Rev. Applied 16, 044023, 2021, doi: 10.1103/PhysRevApplied.16.044023.

[11] A. Pilotto, P. Dollfus, J. Saint-Martin, M.G. Pala, "Full quantum simulation of Shockley–Read–Hall recombination in p-i-n and tunnel diodes", Solid-State Electronics, vol. 198, 108469, 2022, doi: 10.1016/j.sse.2022.108469.

[12] A. Schenk and U. Krumbein, "Coupled defect-level recombination: Theory and application to anomalous diode characteristics", in Journal of Applied Physics 78(5), pp. 3185–3192, 1995, doi: 10.1063/1.360007.

[13] M. Oehme, D. Hähnel, J. Werner, M. Kaschel, O. Kirfel, E. Kasper, J. Schulze, "Si Esaki diodes with high peak to valley current ratios", in Appl. Phys. Lett. 95 (24), 242109, 2009, doi: 10.1063/1.3274136.